AMERICAN SOCIETY FOR MICROBIOLOGY | mBio®

RESEARCH ARTICLE

Preexisting Heterogeneity of Inducible Nitric Oxide Synthase Expression Drives Differential Growth of *Mycobacterium tuberculosis* in Macrophages

Ophélie Rutschmann,[a] Chiara Toniolo,[a] John D. McKinney[a]

[a]School of Life Sciences, Swiss Federal Institute of Technology in Lausanne, Lausanne, Switzerland

ABSTRACT *Mycobacterium tuberculosis* infection is initiated by the inhalation and implantation of bacteria in the lung alveoli, where they are phagocytosed by macrophages. Even a single bacterium may be sufficient to initiate infection. Thereafter, the clinical outcome is highly variable between individuals, ranging from sterilization to active disease, for reasons that are not well understood. Here, we show that the rate of intracellular bacterial growth varies markedly between individual macrophages, and this heterogeneity is driven by cell-to-cell variation of inducible nitric oxide synthase (iNOS) activity. At the single-cell level, iNOS expression fluctuates over time, independent of infection or activation with gamma interferon. We conclude that chance encounters between individual bacteria and host cells randomly expressing different levels of an antibacterial gene can determine the outcome of single-cell infections, which may explain why some exposed individuals clear the bacteria while others develop progressive disease.

IMPORTANCE In this report, we demonstrate that fluctuations in the expression of antimicrobial genes can define how single host cells control bacterial infections. We show that preexisting cell-to-cell variation in the expression of a single gene, that for inducible nitric oxide synthase, is sufficient to explain why some macrophages kill intracellular *M. tuberculosis* while others fail to control bacterial replication, possibly leading to disease progression. We introduce the concept that chance encounters between heterogeneous bacteria and host cells can determine the outcome of a host-pathogen interaction. This concept is particularly relevant for all the infectious diseases in which the number of interacting pathogens and host cells is small at some point during the infection.

KEYWORDS *Mycobacterium tuberculosis*, macrophages, single-cell, heterogeneity, inducible nitric oxide synthase (iNOS), gamma interferon (IFN-γ), time-lapse, microscopy, innate immunity

A *Mycobacterium tuberculosis* infection usually starts when airborne droplets containing one or more bacteria enter an individual's lungs and interact with alveolar macrophages (1). From this initial encounter, outcomes range from sterilization to latent infection or active disease (2). These heterogeneous outcomes may be linked to differences in the evolution of granulomas, the characteristic multicellular structures that form around bacteria in the lungs (3–5). However, clinical studies have shown that some individuals who are heavily exposed to *M. tuberculosis* remain tuberculin skin test negative and presumably uninfected, suggesting that it is possible for the host to suppress or clear the bacteria during the earliest stages of infection (6, 7). Thus, different infection outcomes may depend not only on granuloma evolution at later stages of the disease, but also on differences in the outcomes of interactions between *M. tuberculosis* and host cells during the initial phases of the infection.

Several findings support this hypothesis. During the first few weeks of infection, macrophages control *M. tuberculosis* growth differently due to differences in their metabolism or expression of immune-related genes, such as the gene for inducible nitric oxide synthase

Editor Christina L. Stallings, Washington University School of Medicine in St. Louis

Address correspondence to Chiara Toniolo, chiara.toniolo87@gmail.com.

The authors declare no conflict of interest.

[This article was published on 19 September with errors in some supplemental material citations. The citations were updated in the current version, posted on 7 October 2022.]

Received 5 August 2022
Accepted 30 August 2022
Published 19 September 2022

(iNOS) and genes downstream of NF-κB (8–10). Heterogeneous control of intracellular *M. tuberculosis* growth is observed not only in macrophages of different lineages, but also in homogeneous populations of primary macrophages cultivated *in vitro* (11). However, those previous studies did not distinguish whether cell-to-cell differences in the control of intracellular *M. tuberculosis* depended on different adaptation of infected host cells to the bacteria (12) or on preexisting heterogeneity in the host cells (13). Answering this fundamental question is particularly relevant in the context of tuberculosis, because an infection can start with a single bacterium coming in contact with a single host macrophage (14, 15). Thus, preexisting phenotypic heterogeneity among host cells, or heterogeneous cellular responses to intracellular bacteria, could influence whether an infection progresses or, conversely, the host is able to control and possibly eliminate the pathogen.

In this study, we investigated how preexisting phenotypic diversity in a population of macrophages contributed to the control of intracellular *M. tuberculosis*. To explore the behavior of individual macrophages infected with fluorescently labeled *M. tuberculosis*, we used single-cell time-lapse microscopy, a technique that has been successfully used to assess infection dynamics at the single-cell level and to investigate the links between host cell death and bacterial growth rate (16, 17). We observed that bacteria within the same macrophage displayed more similar growth rates than bacteria in different macrophages, suggesting that some host cells are better than others at controlling *M. tuberculosis* infection. Using fluorescent reporter macrophages, we found that iNOS expression varied between individual macrophages and fluctuated over time. This preexisting heterogeneity of iNOS expression explains the differential control of intracellular *M. tuberculosis* growth even within a clonal population of macrophages. Our findings highlight the importance of considering preexisting phenotypic heterogeneity in host cells when studying the pathophysiology of an infectious disease, as these differences may determine the outcome of the initial encounter between host and pathogen.

RESULTS

Intracellular growth of *M. tuberculosis* and survival of infected host cells are heterogeneous at the single-cell level. We used fluorescence time-lapse microscopy to image individual mouse bone marrow-derived macrophages (BMDMs) infected with green fluorescent protein (GFP)-expressing *Mycobacterium tuberculosis* (Fig. 1A). The total fluorescent area per macrophage measured at 2-h intervals was used as a proxy for the number of intracellular bacteria and to calculate the growth rate of each intracellular microcolony. Macrophages can partially control *M. tuberculosis* growth, as the median growth rate of intracellular bacteria (0.036 per hour, corresponding to a doubling time of 27.8 h) (Fig. 1B) was reduced in comparison to extracellular bacteria growing on the debris of dead cells in the same culture (growth rate of 0.078 per hour, corresponding to a doubling time of 12.8 h) (Fig. 1C). Intracellular bacterial growth was heterogeneous: some intracellular bacteria grew with a growth rate above 0.08 per hour, corresponding to a doubling time of 12.5 h (Fig. 1A, lower panel, and Fig. 1B), while others grew very slowly, with doubling times of more than 1 week (Fig. 1A, upper panel, and Fig. 1B). Over 168 h of continuous imaging, ~60% of infected host cells died at different time points after infection (Fig. 1D). Surprisingly, the fate of individual infected macrophages (death or survival over the 168-h imaging period) did not correlate with the initial bacterial load (Fig. 1E), final bacterial load (Fig. 1F), or growth rate of intracellular *M. tuberculosis* (Fig. 1G; see also Fig. S1 in the supplemental material). Indeed, some macrophages survived even with a bacterial load that was higher than the median bacterial load in macrophages that died (Fig. 1F). It is worth noting, however, that even though no significant trend appeared, a subpopulation of exceptionally fast-growing intracellular bacteria with growth rates greater than 0.8 per hour, corresponding to a doubling time of less than 12.5 h, eventually did kill their host cells (Fig. 1G).

Heterogeneity of intracellular *M. tuberculosis* growth rates is linked to variability in the macrophage population. The observed single-cell heterogeneity in intracellular *M. tuberculosis* growth rates could reflect heterogeneity in the bacterial population (some bacteria resist macrophage-imposed stresses better than others) or variability in the

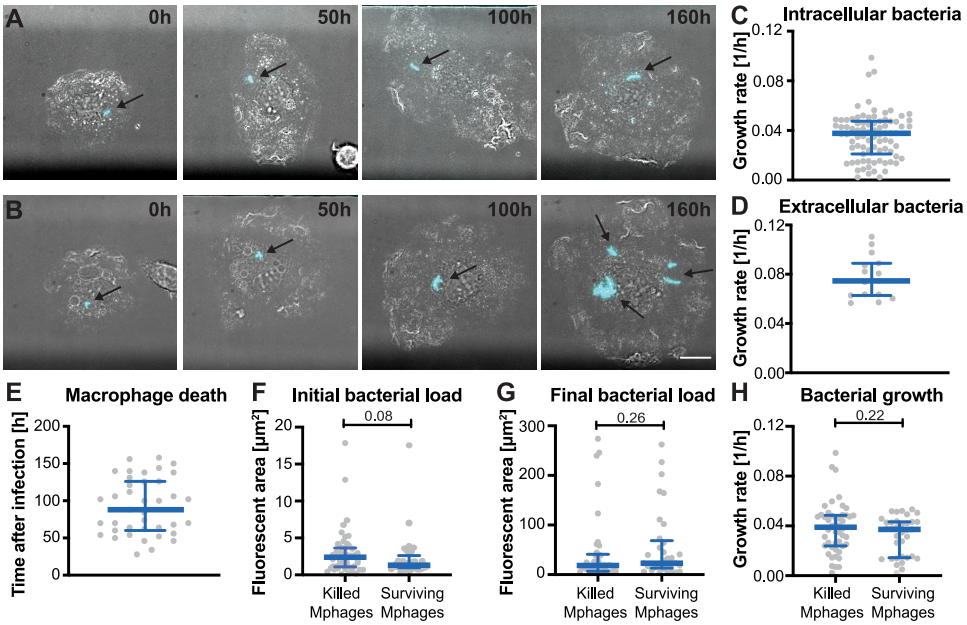

FIG 1 Intracellular growth of *M. tuberculosis* and survival of infected host cells are heterogeneous at the single-cell level. Murine BMDMs were infected with GFP-expressing *M. tuberculosis* and imaged by time-lapse microscopy at 2-h intervals for 168 h. (A) Example of an infected macrophage in which bacteria (cyan) grew slowly (doubling time, >168 h). (B) Example of an infected macrophage in which bacteria grew quickly (doubling time, <20 h). (C) Growth rates of intracellular *M. tuberculosis*. Each symbol represents a bacterial microcolony inside a single infected macrophage. (D) Growth rates of extracellular *M. tuberculosis*. Each symbol represents a single extracellular bacterial microcolony. (E) Survival time of infected macrophages that died before the end of the experiment. Each symbol represents a single macrophage. Survival time was calculated from the frame when initial infection occurred to the frame when death occurred. (F to H) Initial bacterial load (F), final bacterial load (G), and growth rate of intracellular bacteria (H) for macrophages that died during the experiment (killed Mphages) or macrophages that survived until the end of the experiment (surviving Mphages). Each symbol represents a single infected macrophage. Blue lines indicate median values and interquartile ranges. Scale bar, 10 μm. *P* values were calculated using a Mann-Whitney test.

macrophage population (some cells control *M. tuberculosis* growth better than others). To address this question, we coinfected BMDMs with two fluorescently labeled *M. tuberculosis* strains expressing either constitutive GFP or tdTomato (Fig. 2A), which displayed similar intracellular growth rates (see Fig. S2). BMDMs infected with one bacterial cell of each color were imaged by time-lapse microscopy, and growth rates were calculated independently for intracellular bacterial microcolonies originating from a GFP$^+$ or tdTomato$^+$ bacterium. This approach permitted the comparison of two microcolonies (one GFP$^+$, one tdTomato$^+$) growing inside the same macrophage, or of two microcolonies growing in different macrophages (Fig. 2B). If variability in the macrophage population contributes to heterogeneity in intracellular bacterial growth rates, then two microcolonies in the same macrophage should behave more similarly than two microcolonies in different macrophages. We tested this hypothesis in unactivated macrophages and in macrophages preactivated with gamma interferon (IFN-γ), a cytokine that induces the expression of antibacterial host defense mechanisms (18) (see Fig. S2C). We found that the difference in growth rates between two intracellular bacterial microcolonies was smaller, on average, if they were in the same host cell than if they were in different cells, in both unactivated and IFN-γ-activated macrophages (Fig. 2C). These results suggest that some individual host cells control *M. tuberculosis* growth better than others, irrespective of their activation status.

Single-cell variation in nitric oxide production by macrophages drives heterogeneous growth of intracellular *M. tuberculosis*. Nitric oxide production by iNOS is one of the IFN-γ-induced mechanisms that macrophages use to control intracellular growth of *M. tuberculosis* (19, 20). We hypothesized that cell-to-cell differences in iNOS activity might explain why some host cells control *M. tuberculosis* growth better than others. We tested this hypothesis by coinfecting BMDMs with single GFP$^+$ and tdTomato$^+$ bacteria while inhibiting iNOS activity with aminoguanidine (Fig. 2C; see also Fig. S3A). In both unactivated and IFN-γ-activated BMDMs treated with aminoguanidine, intermacrophage

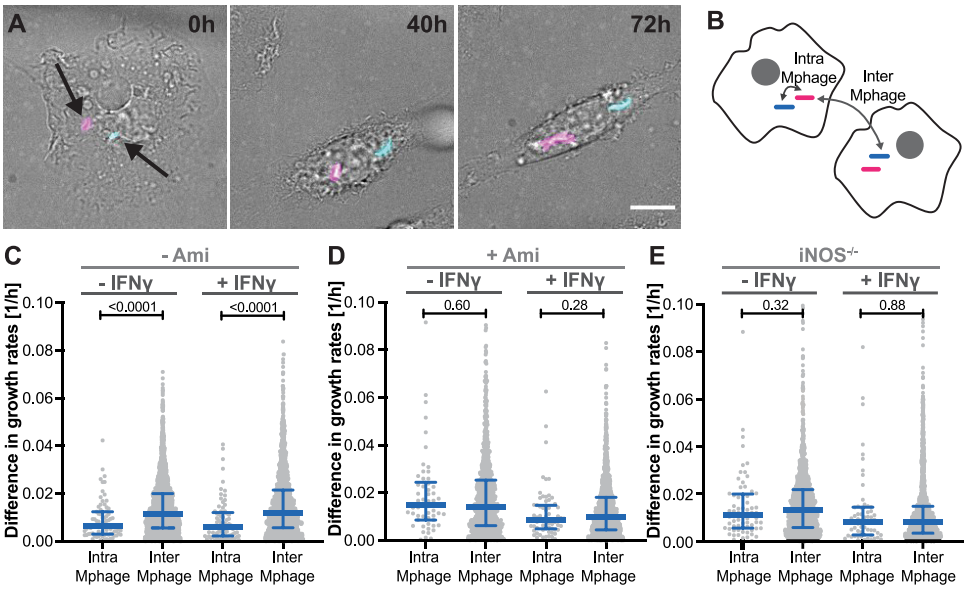

FIG 2 Single-cell variability of macrophage nitric oxide production drives heterogeneous growth of intracellular *M. tuberculosis*. Murine bone marrow-derived macrophages were simultaneously infected with *M. tuberculosis* strains expressing GFP or tdTomato and imaged by time-lapse microscopy at 1-h or 2-h intervals for 72 h. (A) Representative time-lapse images of a macrophage coinfected with GFP-expressing (cyan) and tdTomato-expressing (magenta) *M. tuberculosis*. (B) Schematic representation of the experimental design. The growth rates of two bacterial microcolonies (one green, one red) inside the same macrophage (intra-Mphage) or in two different macrophages (inter-Mphage) were compared. For calculation of intermacrophage differences in growth rate, each GFP-expressing bacterium was compared to all tdTomato-expressing bacteria not in the same macrophage. (C to E) Differences in growth rates between two bacterial microcolonies inside the same macrophage or in two different macrophages. Each symbol represents the difference in growth rates between one green and one red bacterium in unactivated or preactivated wild-type macrophages that were untreated (C), treated with aminoguanidine to inhibit nitric oxide production (D), or in untreated iNOS$^{-/-}$ macrophages (E). Blue lines indicate median values and interquartile ranges. Scale bar, 10 μm. *P* values were calculated using a Mann-Whitney test.

and intramacrophage differences in bacterial growth rates were not significantly different (Fig. 2D). This suggests that, when iNOS activity is inhibited, all macrophages control *M. tuberculosis* growth about equally well. Consistent with this hypothesis, we found that intermacrophage and intramacrophage bacterial growth rates were not significantly different in BMDMs from iNOS$^{-/-}$ mice. This observation held true in both unactivated and IFN-γ-activated iNOS$^{-/-}$ BMDMs (Fig. 2E). Despite inhibition or lack of iNOS activity, IFN-γ activation was still effective in reducing intracellular bacterial growth (see Fig. S2C), presumably due to other IFN-γ-activated defenses, such as IRGM1 (21). We conclude that cell-to-cell variation in iNOS activity is linked to the control of intracellular *M. tuberculosis* growth in macrophages, irrespective of their activation status.

Single-cell variability of macrophage iNOS expression in a reporter cell line contributes to heterogeneous growth of intracellular *M. tuberculosis*. To further investigate the link between cell-to-cell heterogeneity of iNOS gene expression and intracellular *M. tuberculosis* growth, we used RAW 264.7 reporter macrophages that expressed yellow fluorescent protein (YFP) from a copy of the iNOS promoter stably integrated in the genome (22). In these macrophages, iNOS-YFP is expressed at low basal levels in unactivated cells and is strongly induced upon activation with IFN-γ (Fig. 3A; see also Fig. S4).

To verify that iNOS-YFP expression was indeed linked to nitric oxide production, we flow-sorted the macrophages into low- and high-fluorescence subpopulations (Fig. 3A) and performed a Griess assay to measure the concentration of reactive nitrogen species (RNS) in the culture supernatants 24 h after sorting. iNOS-YFP^{low} cells produced less RNS than iNOS-YFP^{high} cells in both unactivated and IFN-γ-activated samples, confirming that iNOS-YFP expression is linked to RNS production (Fig. 3B).

We infected four flow-sorted subpopulations of macrophages ($\pm$ IFN-γ iNOS-YFP^{low} and $\pm$ IFN-γ iNOS-YFP^{high}) with tdTomato-expressing *M. tuberculosis* and used time-lapse microscopy to measure the growth rates of bacterial microcolonies within individual macrophages. In

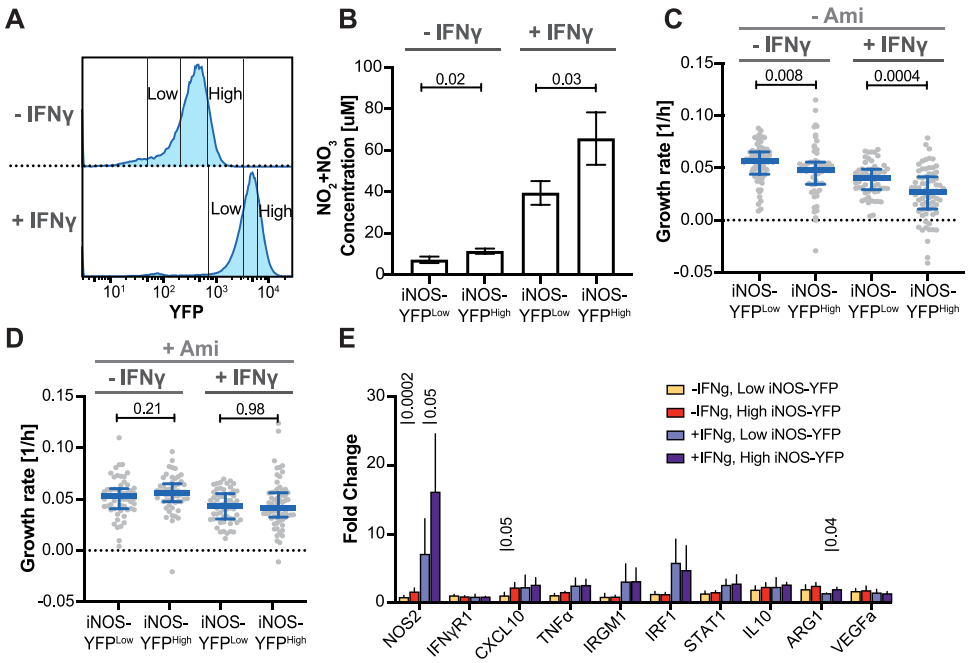

FIG 3 Single-cell variability of iNOS expression by macrophages contributes to heterogeneous growth rates of intracellular *M. tuberculosis*. Unactivated (−IFN-γ) and activated (+IFN-γ) RAW 264.7 macrophages that stably expressed YFP from the iNOS transcriptional promoter were flow-sorted into low- and high-fluorescence subpopulations prior to analysis. (A) Flow cytometry fluorescence profiles of iNOS-YFP-expressing macrophages. High-YFP and low-YFP gates are indicated. (B) The Griess assay was used to measure the cumulative concentration of reactive nitrogen species (NO_2 + NO_3) in the supernatants of macrophage subpopulations 24 h after sorting. *P* values were calculated using Student's *t* test. (C and D) Growth rates of intracellular *M. tuberculosis* in flow-sorted macrophage subpopulations were measured by time-lapse microscopy during 72 h. Macrophages were untreated (C) or treated with aminoguanidine to inhibit nitric oxide production (D). Each symbol represents a bacterial microcolony inside a single macrophage. Blue lines indicate median values and interquartile ranges. *P* values were calculated using a Mann-Whitney test. (E) Expression levels of selected genes involved in the IFN-γ response or linked to macrophage polarization in flow-sorted macrophage subpopulations. Relative expression (fold change) was normalized to an unactivated and unsorted sample. NOS2, IFN-γR1, CXCL10, IRGM1, IRF1, and STAT1 are involved in the IFN-γ response and, along with tumor necrosis factor α (TNF-α), are markers for M1 polarization. VEGFa and ARG1 are markers for M2 polarization. *P* values were calculated using Student's *t* test (*P* values of >0.05 are not shown).

both unactivated and IFN-γ-activated macrophage subpopulations, iNOS-YFP^{high} cells controlled bacterial growth significantly better than iNOS-YFP^{low} cells (Fig. 3C). This difference was abolished when iNOS activity was inhibited with aminoguanidine, confirming that it is dependent on nitric oxide production (Fig. 3D; see also Fig. S3B). As we observed in infected BMDMs (see Fig. S2C), when iNOS activity was inhibited, IFN-γ-activated RAW 264.7 macrophages still controlled *M. tuberculosis* growth better than unactivated macrophages (Fig. 3D). For all conditions tested, the survival rate of infected macrophages was similar over the course of the experiments, indicating that the observed differences in bacterial growth rates were not due to differences in host cell viability (see Fig. S5).

iNOS expression is not linked to differences in macrophage polarization or expression of other IFN-γ-regulated genes. We investigated whether cell-to-cell differences in iNOS expression are linked to macrophage polarization or single-cell variability in IFN-γ-responsive gene expression by quantitative real-time PCR (qRT-PCR) analysis of unactivated or IFN-γ-activated iNOS-YFP^{low} and iNOS-YFP^{high} cells. These experiments confirmed that iNOS mRNA expression correlates with iNOS-YFP fluorescence levels (Fig. 3E). However, we did not observe any differences between iNOS-YFP^{high} and iNOS-YFP^{low} macrophages in the expression of other genes associated with macrophage polarization or the IFN-γ response (Fig. 3E).

iNOS expression and RNS production fluctuate over time. The observation that individual macrophages express iNOS-YFP at different levels prompted us to ask whether these cell-to-cell differences are stable or unstable over time. We used flow cytometry to measure fluorescence levels in flow-sorted macrophage subpopulations 0, 24, 48, 72, and

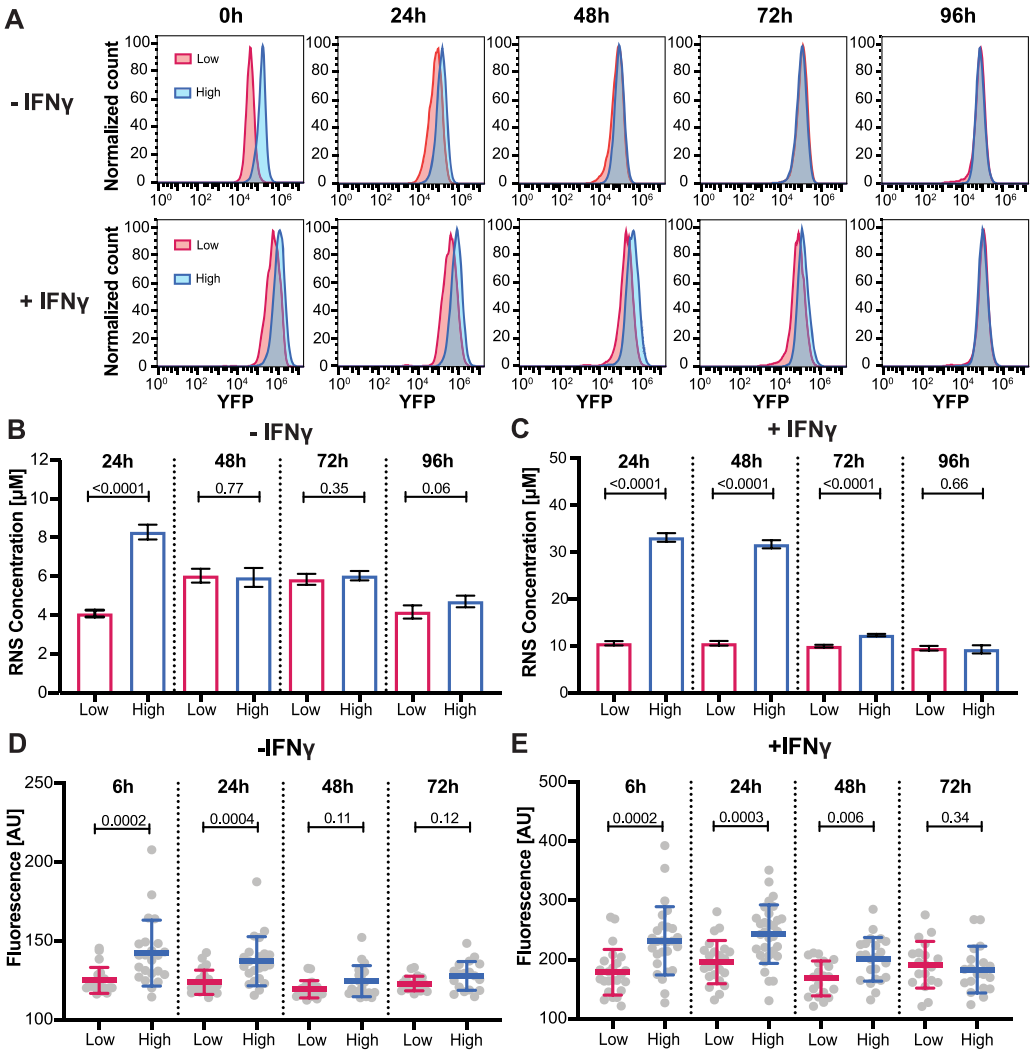

FIG 4 iNOS expression and RNS production fluctuate over time. Unactivated (−IFN-γ) and activated (+IFN-γ) RAW 264.7 macrophages that stably expressed YFP from the iNOS transcriptional promoter were flow-sorted into low- and high-fluorescence subpopulations prior to analysis. (A) Flow cytometry fluorescence profiles of iNOS-YFP-expressing macrophages 6, 24, 48, 72, and 96 h after sorting. (B and C) RNS concentrations in the supernatant of unactivated (B) and IFN-γ-activated (C) iNOS-YFP-expressing macrophages 24, 48, 72, and 96 h after sorting. *P* values were calculated using Student's *t* test. (D and E) Single infected macrophages were identified and tracked using time-lapse microscopy. Shown are the fluorescence of *M. tuberculosis*-infected unactivated (D) and IFN-γ-activated (E) iNOS-YFP-expressing macrophages 6, 24, 48, and 72 h after sorting as measured by microscopy. Each symbol represents a single infected macrophage. Blue lines indicate median values and interquartile ranges. *P* values were calculated using a Mann-Whitney test.

96 h after sorting. This analysis revealed that the iNOS-YFP^{low} and iNOS-YFP^{high} subpopulations were not stable over time and slowly converged toward each other in both unactivated and IFN-γ-activated samples (Fig. 4A). Convergence of the iNOS-YFP^{low} and iNOS-YFP^{high} subpopulations was faster in the unactivated samples than in the IFN-γ-activated samples. To confirm that the fluctuations in iNOS-YFP expression reflected changes in RNS production, we performed a Griess assay to measure levels of RNS secreted by iNOS-YFP^{low} and iNOS-YFP^{high} subpopulations 24, 48, 72, and 96 h after sorting. The amount of RNS secreted by the different subpopulations also fluctuated over time and converged within a similar time frame as iNOS-YFP expression for both unactivated and IFN-γ-activated samples (Fig. 4B and C).

Finally, to assess the impact of infection on the fluctuation of iNOS-YFP expression at the single-cell level, we infected flow-sorted subpopulations of macrophages with tdTomato-expressing *M. tuberculosis* and tracked single infected cells over 72 h using time-lapse fluorescence microscopy. As observed in our population-based experiments, we found that iNOS-YFP expression levels fluctuated in single cells and macrophages sorted into iNOS-YFP^{low} and

iNOS-YFP^{high} populations converged over time and stabilized around the average level of gene expression found in the macrophage population prior to sorting (Fig. 4D and E; see also Fig. S6). These results confirmed that iNOS-YFP expression fluctuates independently of infection or IFN-γ activation, although activation may influence the time scale of these fluctuations.

Despite the observed fluctuations in iNOS-YFP expression over time, we were able to measure significant differences in bacterial growth rates between iNOS-YFP^{high} and iNOS-YFP^{low} cells over the course of our experiments. These observations suggested that early exposure to different concentrations of intracellular RNS may be sufficient to drive differences in bacterial growth rates at early as well as late time points. We tested this hypothesis by comparing bacterial growth rates in unactivated iNOS-YFP^{high} and iNOS-YFP^{low} macrophages between 0 and 36 h and between 36 and 72 h. We found that intracellular bacterial growth rates were significantly different between iNOS-YFP^{high} and iNOS-YFP^{low} subpopulations during both the early and late time intervals (see Fig. S7), suggesting that differences in iNOS gene expression, even when limited to the early stages of infection, can have a long-lasting impact on bacterial growth rates.

DISCUSSION

During the course of an infection, *M. tuberculosis* encounters heterogeneous niches ranging from different intracellular compartments to different types of cells and lesions (2, 23). This interplay between bacteria and heterogeneous host environments likely plays a role in determining the outcome of infection, ranging from disease progression to sterilization.

Here, we focused on the initial phases of an *M. tuberculosis* infection, during which small numbers of bacteria interact with individual host cells, to determine whether preexisting phenotypic heterogeneity in macrophages could drive differential growth of intracellular *M. tuberculosis*, potentially leading to different infection outcomes. We observed that individual cells can express different levels of iNOS within a clonal population of macrophages; this heterogeneity was not linked to differences in macrophage polarization, nor to the expression of other IFN-γ-related genes. Macrophages that expressed higher level of iNOS at the time of initial infection were more effective in controlling intracellular *M. tuberculosis* growth, suggesting that differences in expression levels of a single host antimicrobial gene could be sufficient to explain cell-to-cell variation in the control of intracellular bacteria. Our *in vitro* observations complemented a recent study showing that different populations of macrophages expressing different levels of iNOS coexist in the lungs of mice infected with *M. tuberculosis* and expression of iNOS correlates with expression of the bacterial stress marker HspX (10). Although the role of iNOS in protection against tuberculosis in humans remains controversial, expression of iNOS has recently been observed in lung sections from tuberculosis patients and in explanted human alveolar macrophages infected with *M. tuberculosis* (24, 25). Interestingly, human alveolar macrophages infected with *M. tuberculosis* show significant heterogeneity in the expression of several proinflammatory markers, including iNOS, which is correlated to their intracellular *M. tuberculosis* load (25). These studies suggest that heterogeneity in iNOS expression could have a role in disease progression *in vivo*.

Our observations that iNOS expression fluctuates in single macrophages and that flow-sorted iNOS-YFP^{high} and iNOS-YFP^{low} subpopulations converge toward an average level of iNOS expression over time (Fig. 4) are consistent with previous evidence that gene expression may be essentially stochastic at the single-cell level. According to this framework, genes are transcribed in bursts of variable intensity that occur at random time intervals (26–29). Based on these observations, we hypothesize that in individual macrophages iNOS expression might occur in bursts separated by silent intervals of variable duration. This model could explain our observation that flow-sorted subpopulations of iNOS-YFP^{high} and iNOS-YFP^{low} macrophages converged over time and eventually stabilized around the average level of iNOS expression found in the population prior to sorting. However, we cannot exclude that fluctuations in iNOS expression might reflect other mechanisms, such as cell cycle-dependent changes in gene expression or modifications in chromatin accessibility (30).

Cell-to-cell variation in iNOS expression seems to account for most of the intermacrophage heterogeneity in *M. tuberculosis* growth rates observed in our experiments. However, we also found that two bacteria growing inside the same host cell may exhibit different growth rates. Intramacrophage differences in *M. tuberculosis* growth rates could reflect occupancy of more or less permissive intracellular compartments by individual bacteria within the same macrophage (31–38). Alternatively, heterogeneous infection outcomes could also originate from the pathogen itself. Phenotypic heterogeneity in clonal bacterial populations is well documented and can be amplified by host stress, resulting in differences in bacterial fitness (12, 39–42). Cell-to-cell differences in the expression of bacterial virulence factors could also impact bacterial growth indirectly by driving different host-cell responses (43). It is thus likely that heterogeneous single-cell growth of intracellular bacteria is due to the interplay of different host and bacterial factors.

Our finding that preexisting heterogeneity in host cells can have an impact on the growth of intracellular *M. tuberculosis* is particularly relevant for tuberculosis, because even a single bacterium infecting a single permissive host cell may be sufficient to initiate an infection (14, 15). Macrophages have been reported to exhibit heterogeneity in the expression of many immune-related genes due to factors such as circadian rhythm, environmental variation, or age of the host, which could all impact how they respond to an initial infection (44–47). Our results suggest that differences in the expression of even a single antimicrobial gene, such as the gene for iNOS, could be sufficient to influence the outcome of infection. This conclusion could potentially be extended to any disease where the number of interacting host cells and bacteria is small at some stage of the infection (48). In such cases, chance encounters of the pathogen with host cells expressing different levels of antibacterial defense mechanisms could determine whether infection is controlled or progresses to active disease.

MATERIALS AND METHODS

Bone marrow-derived macrophages. BMDMs were differentiated from frozen bone marrow stocks extracted from femurs of wild-type C57BL/6 mice or iNOS$^{-/-}$ mice (B6.129P2-Nos2tm1Lau/J mice from Jackson Laboratories, catalog number 002609). The bone marrow was cultured in petri dishes in BMDM differentiation medium (Dulbecco's modified Eagle's medium [DMEM] with 10% fetal bovine serum [FBS], 1% sodium pyruvate, 1% GlutaMax, and 20% L929 cell-conditioned medium [as a source of granulocyte-macrophage colony-stimulating factor]) for 7 days. The adherent cells were then gently lifted from the plate using a cell scraper and resuspended in BMDM culture medium (DMEM with 5% FBS, 1% sodium pyruvate, 1% GlutaMax, and 5% L929 cell-conditioned medium). The macrophages were then seeded in 35-mm ibidi μ-dishes or in 4-compartment ibidi μ-dishes and allowed to adhere for 4 h at 37°C, 5% CO_2 before use.

RAW 264.7 iNOS-YFP macrophage cell line. RAW 264.7 macrophages stably expressing YFP from a copy of the iNOS transcriptional promoter (22) were cultured in DMEM with 10% FBS, 1% Glutamax, and 1% sodium pyruvate at 37°C, 5% CO_2. The macrophages were passaged every 3 days at a 1:4 ratio by gently lifting them off the culture flask with a cell scraper.

***M. tuberculosis* strains.** GFP- and tdTomato-expressing *M. tuberculosis* Erdman strains were inoculated from frozen glycerol stocks in Middlebrook 7H9 (Difco) supplemented with 10% albumin-dextrose-saline (ADS), 0.5% glycerol, and 0.02% tyloxapol and cultured at 37°C with shaking.

Flow sorting of RAW 264.7 iNOS-YFP reporter macrophages. RAW 264.7 iNOS-YFP macrophages were detached from culture flasks with 10 mM EDTA. When required, macrophages were activated 24 h before detaching with 100 U/mL IFN-γ. The cells were then collected by centrifugation, resuspended in fluorescence-activated cell sorting (FACS) buffer (phosphate-buffered saline [PBS] with 1 mM EDTA), and sorted using a FACSaria Fusion system (the gating strategy is shown in Fig. S3 in the supplemental material). Sorted cells were collected, resuspended in DMEM with 10% FBS, 1% Glutamax, and 1% sodium pyruvate, seeded in μ-dishes, and allowed to adhere for at least 4 h before use.

Macrophage infections. For infection, 1 mL of *M. tuberculosis* culture at an optical density at 600 nm (OD_{600}) of 0.5 was pelleted and resuspended in 200 μL of macrophage medium. Bacteria were passed through a 5-μm filter to eliminate aggregates. The resulting single-cell suspension was used to infect BMDMs or RAW 264.7 iNOS-YFP macrophages at a multiplicity of infection (MOI) of 1:1. When two fluorescent strains of *M. tuberculosis* were used simultaneously, both were added at an MOI of 1:1. After 4 h of infection, macrophages were washed extensively with macrophage medium to remove extracellular bacteria. When required, 100 U/mL IFN-γ was added to the macrophage medium 24 h before infection and maintained during the duration of the experiment. When required, 500 μM aminoguanidine was added to the culture medium at the time of infection and maintained thereafter.

Time-lapse microscopy of macrophages infected with *M. tuberculosis*. Infected BMDMs and RAW 264.7 iNOS-YFP macrophages were imaged with a DeltaVision microscope and a Nikon Ti2 microscope, respectively. A stage-top incubator (Okolab) was used to maintain the cells at 37°C in a humidified environment. Air mixed to 5% CO_2 was supplied using an Okolab gas mixer. Infected BMDMs were randomly selected and imaged for up to 168 h. Macrophage medium was refreshed every 3 days via custom

tubing connected to the lid of the ibidi μ-dish. Infected BMDMs were imaged using a 60× oil-immersion objective at 2-h intervals; 3 × 1 μm *z*-stacks were acquired for each point. Bacteria were identified by fluorescence emission on the green (GFP) or red (tdTomato) channel using fluorescein isothiocyanate (excitation [Ex] 490/20, emission [Em] 525/36) and tetramethyl rhodamine isocyanate (Ex 555/25, Em 605/52) filters, respectively. Infected RAW 264.7 iNOS-YFP macrophages were imaged for 72 h using a 40× air objective at 1-h intervals; 3 × 1 μm or 5 × 1 μm *z*-stacks were acquired for each point. iNOS-YFP levels were quantified and tdTomato-expressing bacteria were imaged using GFP (Em 480/30, Ex 535/45) and mCherry (Em 560/40, Ex 635/60) dichroic filters, respectively. For both BMDMs and RAW 264.7 iNOS-YFP macrophages, at least 25 infected cells were imaged per condition.

Quantification of reactive nitrogen species (RNS) in cell culture medium. BMDMs and RAW 264.7 iNOS-YFP macrophages were seeded in triplicates in 96-well plates with 100 μL of their respective culture medium at a concentration of 10^6 cells/mL. When required, 100 U/mL IFN-γ or 500 μM aminoguanidine was added to the culture medium. After 24 h of incubation at 37°C, 5% CO_2, 80 μL of culture supernatant was collected and centrifuged at 10,000 × *g* for 10 min. The concentration of RNS in the supernatant was measured using a nitrate/nitrite colorimetric assay kit (Abnova), as described by the manufacturer. Since RAW 264.7 macrophages divide approximately every 24 h, a different seeding strategy was used for time course experiments with these cells. Each population of flow-sorted RAW 264.7 iNOS-YFP macrophages was seeded in 4 wells of a 96-well plate at four different concentrations (10^6, 0.5 × 10^6, 0.25 × 10^6, or 0.125 × 10^6 cells/mL, all in 100 μL of medium) and measured at 24, 48, 72, and 96 h after sorting. This seeding strategy ensured that the samples used for different time points reached approximately the same number of cells. The plates were incubated at 37°C, 5% CO_2 between the different time points. When required, 100 U/mL of IFN-γ was added to the medium of the cells directly after sorting.

Quantitative real-time PCR. Unactivated or preactivated (+100 U/mL IFN-γ) RAW 264.7 iNOS-YFP macrophages were sorted as described above. Directly after sorting, the macrophages were collected by centrifugation and lysed, and RNA was extracted using a Qiagen RNeasy micro kit plus according to the manufacturer's instructions. DNase treatment was performed directly on the column during RNA extraction. The RNA was then reverse-transcribed with random hexamers using the SuperScript IV first-strand synthesis system (ThermoFisher). qRT-PCR mixtures were prepared using the SYBRGreen PCR master mix (Applied Biosystems) with 1 μM primers and 2 μL of cDNA. Reactions were run on an ABI Prism 7900HT sequence detection system (Applied Biosystems). Amplicon specificity was confirmed by melting curve analysis. Primer sequences were obtained from Origene. Primers were synthesized by Microsynth, Switzerland (see Table S1).

Flow cytometry time course. FACS-sorted unactivated or preactivated (+100 U/mL IFN-γ) RAW 264.7 iNOS-YFP macrophage subpopulations were seeded following the same seeding strategy described for the time course experiments to quantify RNS. For each subpopulation, 5 wells of a 24-well plate were seeded with 350 μL of cells at 2 × 10^6, 10^6, 0.5 × 10^6, 0.25 × 10^6, or 0.125 × 10^6 cells/mL and analyzed by flow cytometry at 4, 24, 48, 72, and 96 h after sorting. The plates were incubated at 37°C, 5% CO_2 between the different time points. When required, 100 U/mL IFN-γ was added to the medium of the cells directly after sorting. For analysis by flow cytometry, the cells were detached using trypsin, collected by centrifugation, resuspended in PBS plus 1 mM EDTA, and analyzed using a BD Accuri C6 flow cytometer.

Image analysis. Image analysis was performed using the FIJI version of the ImageJ software (49). All infected macrophages that survived for at least 24 h of imaging were analyzed. If a macrophage divided during the experiment, the daughter cell containing the bacteria was selected for continued analysis. If the bacterial microcolony was split between the two daughter cells, the analysis was stopped at this time point. All of the macrophages were imaged until the end of the experiment or until their death. The *z*-stacks acquired were projected into one image using a maximum intensity projection. A background subtraction was performed by subtracting from the fluorescence images a copy of the same images on which a Gaussian blur of 100-μm radius had been applied. Regions of interest corresponding to individual macrophages were manually drawn onto the phase images and transferred to the fluorescence images. A manual threshold was set on the fluorescence channel to segment the bacteria. The area above the threshold inside single macrophages was measured and used as a proxy for the number of intracellular bacteria for each time point. To quantify the growth rate of the intracellular bacteria, an exponential curve was fitted to the data. A similar method was used to measure the growth rate of bacteria identified as extracellular in BMDM infection experiments. Similarly, iNOS-YFP expression levels were quantified for each frame by transferring the manually drawn regions of interest corresponding to individual infected macrophages to the GFP fluorescence images. The average fluorescence intensity was measured for each individual macrophage and used as a proxy for iNOS-YFP expression levels. Cell death was identified using bright-field images. When macrophages die, they change shape (shrink), lose membrane integrity, and stop moving. Death events were identified by examining the subsequent time-lapse images for each cell (see Fig. S1). The time of death was manually annotated as the first time point at which death was observed. Out-of-focus images were manually excluded from analysis.

Resource availability. Further information and requests for resources and reagents should be directed to and will be fulfilled by the corresponding author, Chiara Toniolo.

Materials availability. This study did not generate new unique reagents.

Data and code availability. Any additional information required to reanalyze the data reported in this paper are available from the corresponding author upon request.

SUPPLEMENTAL MATERIAL

Supplemental material is available online only.

FIG S1, PDF file, 2.2 MB.

FIG S2, PDF file, 0.5 MB.

FIG S3, PDF file, 0.4 MB.
FIG S4, PDF file, 0.5 MB.
FIG S5, PDF file, 0.4 MB.
FIG S6, PDF file, 0.4 MB.
FIG S7, PDF file, 0.4 MB.
TABLE S1, DOCX file, 0.01 MB.

ACKNOWLEDGMENTS

This work was supported by a grant to J.D.M. from the Swiss National Science Foundation (310030_207717). C.T. was supported by funding from the European Union's Horizon 2020 Research and Innovation program under Marie Skłodowska-Curie grant agreement 665667. This work was supported in part using the resources and services of the Flow Cytometry Core Facility at the School of Life Sciences of EPFL. We also thank Daniel Sage for help with image analysis and Carl Nathan for providing the RAW 264.7 iNOS-YFP reporter macrophages used in this study.

O.R. contributed Conceptualization, Investigation, Data curation, Writing – original draft, Writing – review & editing, Visualization. C.T. contributed Conceptualization, Investigation, Data Curation, Writing – original draft, Writing – review & editing, Visualization, Supervision. J.D.M. contributed Conceptualization, Writing – review & editing, Supervision, Funding Acquisition.

We declare no competing interests.

REFERENCES

1. Cohen SB, Gern BH, Delahaye JL, Adams KN, Plumlee CR, Winkler JK, Sherman DR, Gerner MY, Urdahl KB. 2018. Alveolar macrophages provide an early Mycobacterium tuberculosis niche and initiate dissemination. Cell Host Microbe 24:439–446.e4. https://doi.org/10.1016/j.chom.2018.08.001.
2. Cadena AM, Fortune SM, Flynn JL. 2017. Heterogeneity in tuberculosis. Nat Rev Immunol 17:691–702. https://doi.org/10.1038/nri.2017.69.
3. Lin PL, Ford CB, Coleman MT, Myers AJ, Gawande R, Ioerger T, Sacchettini J, Fortune SM, Flynn JL. 2014. Sterilization of granulomas is common in active and latent tuberculosis despite within-host variability in bacterial killing. Nat Med 20:75–79. https://doi.org/10.1038/nm.3412.
4. Martin CJ, Cadena AM, Leung VW, Lin PL, Maiello P, Hicks N, Chase MR, Flynn JL, Fortune SM. 2017. Digitally barcoding Mycobacterium tuberculosis reveals in vivo infection dynamics in the macaque model of tuberculosis. mBio 8:e00312-17. https://doi.org/10.1128/mBio.00312-17.
5. Marakalala MJ, Raju RM, Sharma K, Zhang YJ, Eugenin EA, Prideaux B, Daudelin IB, Chen P-Y, Booty MG, Kim JH, Eum SY, Via LE, Behar SM, Barry CE, Mann M, Dartois V, Rubin EJ. 2016. Inflammatory signaling in human tuberculosis granulomas is spatially organized. Nat Med 22:531–538. https://doi.org/10.1038/nm.4073.
6. Houk VN, Baker JH, Sorensen K, Kent DC. 1968. The epidemiology of tuberculosis infection in a closed environment. Arch Environ Health 16:26–35. https://doi.org/10.1080/00039896.1968.10665011.
7. Simmons JD, Stein CM, Seshadri C, Campo M, Alter G, Fortune S, Schurr E, Wallis RS, Churchyard G, Mayanja-Kizza H, Boom WH, Hawn TR. 2018. Immunological mechanisms of human resistance to persistent Mycobacterium tuberculosis infection. Nat Rev Immunol 18:575–589. https://doi.org/10.1038/s41577-018-0025-3.
8. Huang L, Nazarova EV, Tan S, Liu Y, Russell DG. 2018. Growth of Mycobacterium tuberculosis in vivo segregates with host macrophage metabolism and ontogeny. J Exp Med 215:1135–1152. https://doi.org/10.1084/jem.20172020.
9. Pisu D, Huang L, Grenier JK, Russell DG. 2020. Dual RNA-Seq of Mtb-infected macrophages in vivo reveals ontologically distinct host-pathogen interactions. Cell Rep 30:335–350.e4. https://doi.org/10.1016/j.celrep.2019.12.033.
10. Pisu D, Huang L, Narang V, Theriault M, Lê-Bury G, Lee B, Lakudzala AE, Mzinza DT, Mhango DV, Mitini-Nkhoma SC, Jambo KC, Singhal A, Mwandumba HC, Russell DG. 2021. Single cell analysis of M. tuberculosis phenotype and macrophage lineages in the infected lung. J Exp Med 218:9. https://doi.org/10.1084/jem.20210615.
11. Bryson BD, Rosebrock TR, Tafesse FG, Itoh CY, Nibasumba A, Babunovic GH, Corleis B, Martin C, Keegan C, Andrade P, Realegeno S, Kwon D, Modlin RL, Fortune SM. 2019. Heterogeneous GM-CSF signaling in macrophages is associated with control of Mycobacterium tuberculosis. Nat Commun 10:e2329. https://doi.org/10.1038/s41467-019-10065-8.
12. Avraham R, Haseley N, Brown D, Penaranda C, Jijon HB, Trombetta JJ, Satija R, Shalek AK, Xavier RJ, Regev A, Hung DT. 2015. Pathogen cell-to-cell variability drives heterogeneity in host immune responses. Cell 162:1309–1321. https://doi.org/10.1016/j.cell.2015.08.027.
13. Gierahn TM, Wadsworth MH, Hughes TK, Bryson BD, Butler A, Satija R, Fortune S, Love JC, Shalek AK. 2017. Seq-Well: portable, low-cost RNA sequencing of single cells at high throughput. Nat Methods 14:395–398. https://doi.org/10.1038/nmeth.4179.
14. Riley RL, Mills CC, Nyka W, Weinstock N, Storey PB, Sultan LU, Riley MC, Wells WF. 1995. Aerial dissemination of pulmonary tuberculosis. A two-year study of contagion in a tuberculosis ward. Am J Epidemiol 142:3–14. https://doi.org/10.1093/oxfordjournals.aje.a117542.
15. Saini D, Hopkins GW, Seay SA, Chen CJ, Perley CC, Click EM, Frothingham R. 2012. Ultra-low dose of Mycobacterium tuberculosis aerosol creates partial infection in mice. Tuberculosis (Edinb) 92:160–165. https://doi.org/10.1016/j.tube.2011.11.007.
16. Lerner TR, Borel S, Greenwood DJ, Repnik U, Russell MR, Herbst S, Jones ML, Collinson LM, Griffiths G, Gutierrez MG. 2017. Mycobacterium tuberculosis replicates within necrotic human macrophages. J Cell Biol 216:583–594. https://doi.org/10.1083/jcb.201603040.
17. Mahamed D, Boulle M, Ganga Y, Mc Arthur C, Skroch S, Oom L, Catinas O, Pillay K, Naicker M, Rampersad S, Mathonsi C, Hunter J, Wong EB, Suleman M, Sreejit G, Pym AS, Lustig G, Sigal A. 2017. Intracellular growth of Mycobacterium tuberculosis after macrophage cell death leads to serial killing of host cells. Elife 6:e22028. https://doi.org/10.7554/eLife.28205.
18. Weiss G, Schaible UE. 2015. Macrophage defense mechanisms against intracellular bacteria. Immunol Rev 264:182–203. https://doi.org/10.1111/imr.12266.
19. Chan J, Xing Y, Magliozzo RS, Bloom BR. 1992. Killing of virulent Mycobacterium tuberculosis by reactive nitrogen intermediates produced by activated murine macrophages. J Exp Med 175:1111–1122. https://doi.org/10.1084/jem.175.4.1111.
20. MacMicking JD, North RJ, LaCourse R, Mudgett JS, Shah SK, Nathan CF. 1997. Identification of nitric oxide synthase as a protective locus against tuberculosis. Proc Natl Acad Sci U S A 94:5243–5248. https://doi.org/10.1073/pnas.94.10.5243.
21. MacMicking JD, Taylor GA, McKinney JD. 2003. Immune control of tuberculosis by IFN-gamma-inducible LRG-47. Science 302:654–659. https://doi.org/10.1126/science.1088063.
22. Beaulieu AM, Rath P, Imhof M, Siddall ME, Roberts J, Schnappinger D, Nathan CF. 2010. Genome-wide screen for Mycobacterium tuberculosis genes that regulate host immunity. PLoS One 5:e15120. https://doi.org/10.1371/journal.pone.0015120.

23. Toniolo C, Rutschmann O, McKinney JD. 2021. Do chance encounters between heterogeneous cells shape the outcome of tuberculosis infections? Curr Opin Microbiol 59:72–78. https://doi.org/10.1016/j.mib.2020.08.008.
24. Cho HJ, Lim YJ, Kim J, Koh WJ, Song CH, Kang MW. 2020. Different macrophage polarization between drug-susceptible and multidrug-resistant pulmonary tuberculosis. BMC Infect Dis 20:81. https://doi.org/10.1186/s12879-020-4802-9.
25. Ufimtseva EG, Eremeeva NI, Umpeleva TV, Vakhrusheva DV, Skornyakov SN. 2021. Mycobacterium tuberculosis load in host cells and the antibacterial activity of alveolar macrophages are linked and differentially regulated in various lung lesions of patients with pulmonary tuberculosis. Int J Mol Sci 22:3452. https://doi.org/10.3390/ijms22073452.
26. McAdams HH, Arkin A. 1997. Stochastic mechanisms in gene expression. Proc Natl Acad Sci U S A 94:814–819. https://doi.org/10.1073/pnas.94.3.814.
27. Elowitz MB, Levine AJ, Siggia ED, Swain PS. 2002. Stochastic gene expression in a single cell. Science 297:1183–1186. https://doi.org/10.1126/science.1070919.
28. Friedman N, Cai L, Xie XS. 2006. Linking stochastic dynamics to population distribution: an analytical framework of gene expression. Phys Rev Lett 97:168302. https://doi.org/10.1103/PhysRevLett.97.168302.
29. Raj A, Peskin CS, Tranchina D, Vargas DY, Tyagi S. 2006. Stochastic mRNA synthesis in mammalian cells. PLoS Biol 4:e309. https://doi.org/10.1371/journal.pbio.0040309.
30. Lannan R, Maity A, Wollman R. 2022. Epigenetic fluctuations underlie gene expression timescales and variability. Physiol Genomics 54:220–229. https://doi.org/10.1152/physiolgenomics.00051.2021.
31. Miller BH, Fratti RA, Poschet JF, Timmins GS, Master SS, Burgos M, Marletta MA, Deretic V. 2004. Mycobacteria inhibit nitric oxide synthase recruitment to phagosomes during macrophage infection. Infect Immun 72:2872–2878. https://doi.org/10.1128/IAI.72.5.2872-2878.2004.
32. Rohde K, Yates RM, Purdy GE, Russell DG. 2007. Mycobacterium tuberculosis and the environment within the phagosome. Immunol Rev 219:37–54. https://doi.org/10.1111/j.1600-065X.2007.00547.x.
33. van der Wel N, Hava D, Houben D, Fluitsma D, van Zon M, Pierson J, Brenner M, Peters PJ. 2007. *M. tuberculosis* and *M. leprae* translocate from the phagolysosome to the cytosol in myeloid cells. Cell 129:1287–1298. https://doi.org/10.1016/j.cell.2007.05.059.
34. Welin A, Lerm M. 2012. Inside or outside the phagosome? The controversy of the intracellular localization of *Mycobacterium tuberculosis*. Tuberculosis (Edinb) 92:113–120. https://doi.org/10.1016/j.tube.2011.09.009.
35. Simeone R, Bobard A, Lippmann J, Bitter W, Majlessi L, Brosch R, Enninga J. 2012. Phagosomal rupture by Mycobacterium tuberculosis results in toxicity and host cell death. PLoS Pathog 8:e1002507. https://doi.org/10.1371/journal.ppat.1002507.
36. Schnettger L, Rodgers A, Repnik U, Lai RP, Pei G, Verdoes M, Wilkinson RJ, Young DB, Gutierrez MG. 2017. A Rab20-dependent membrane trafficking pathway controls M. tuberculosis replication by regulating phagosome spaciousness and integrity. Cell Host Microbe 21:619–628.e5. https://doi.org/10.1016/j.chom.2017.04.004.
37. Bakkum T, Heemskerk MT, Bos E, Groenewold M, Oikonomeas-Koppasis N, Walburg KV, van Veen S, van der Lienden MJC, van Leeuwen T, Haks MC, Ottenhoff THM, Koster AJ, van Kasteren SI. 2020. Bioorthogonal correlative light-electron microscopy of Mycobacterium tuberculosis in macrophages reveals the effect of antituberculosis drugs on subcellular bacterial distribution. ACS Cent Sci 6:1997–2007. https://doi.org/10.1021/acscentsci.0c00539.
38. Lienard J, Nobs E, Lovins V, Movert E, Valfridsson C, Carlsson F. 2020. The Mycobacterium marinum ESX-1 system mediates phagosomal permeabilization and type I interferon production via separable mechanisms. Proc Natl Acad Sci U S A 117:1160–1166. https://doi.org/10.1073/pnas.1911646117.
39. Eldar A, Elowitz MB. 2010. Functional roles for noise in genetic circuits. Nature 467:167–173. https://doi.org/10.1038/nature09326.
40. Bhaskar A, Chawla M, Mehta M, Parikh P, Chandra P, Bhave D, Kumar D, Carroll KS, Singh A. 2014. Reengineering redox sensitive GFP to measure mycothiol redox potential of Mycobacterium tuberculosis during infection. PLoS Pathog 10:e1003902. https://doi.org/10.1371/journal.ppat.1003902.
41. Ackermann M. 2015. A functional perspective on phenotypic heterogeneity in microorganisms. Nat Rev Microbiol 13:497–508. https://doi.org/10.1038/nrmicro3491.
42. Manina G, Dhar N, McKinney JD. 2015. Stress and host immunity amplify Mycobacterium tuberculosis phenotypic heterogeneity and induce nongrowing metabolically active forms. Cell Host Microbe 17:32–46. https://doi.org/10.1016/j.chom.2014.11.016.
43. Raffetseder J, Iakobachvili N, Loitto V, Peters PJ, Lerm M. 2019. Retention of EsxA in the capsule-like layer of Mycobacterium tuberculosis is associated with cytotoxicity and is counteracted by lung surfactant. Infect Immun 87:e00803-18. https://doi.org/10.1128/IAI.00803-18.
44. Keller M, Mazuch J, Abraham U, Eom GD, Herzog ED, Volk HD, Kramer A, Maier B. 2009. A circadian clock in macrophages controls inflammatory immune responses. Proc Natl Acad Sci U S A 106:21407–21412. https://doi.org/10.1073/pnas.0906361106.
45. Lafuse WP, Rajaram MVS, Wu Q, Moliva JI, Torrelles JB, Turner J, Schlesinger LS. 2019. Identification of an increased alveolar macrophage subpopulation in old mice that displays unique inflammatory characteristics and is permissive to Mycobacterium tuberculosis infection. J Immunol 203:2252–2264. https://doi.org/10.4049/jimmunol.1900495.
46. Melo EM, Oliveira VLS, Boff D, Galvão I. 2021. Pulmonary macrophages and their different roles in health and disease. Int J Biochem Cell Biol 141:106095. https://doi.org/10.1016/j.biocel.2021.106095.
47. Bain CC, MacDonald AS. 2022. The impact of the lung environment on macrophage development, activation and function: diversity in the face of adversity. Mucosal Immunol 15:223–234. https://doi.org/10.1038/s41385-021-00480-w.
48. Moxon R, Kussell E. 2017. The impact of bottlenecks on microbial survival, adaptation, and phenotypic switching in host-pathogen interactions. Evolution 71:2803–2816. https://www.jstor.org/stable/48575233.
49. Schindelin J, Arganda-Carreras I, Frise E, Kaynig V, Longair M, Pietzsch T, Preibisch S, Rueden C, Saalfeld S, Schmid B, Tinevez J-Y, White DJ, Hartenstein V, Eliceiri K, Tomancak P, Cardona A. 2012. FiJi. Nat Methods 9:676–682. https://doi.org/10.1038/nmeth.2019.